Optics Letters

# Shape-controllable, bottom-up fabrication of microlens using oblique angle deposition

Hee Ju Choi,[1] Eun Kyu Kang,[2] Gun Wu Ju,[2] Young Min Song,[2] and Yong Tak Lee[2,*]

[1]Department of Physics and Photon Science, Gwangju Institute of Science and Technology, Gwangju 500-712, South Korea
[2]School of Electrical Engineering and Computer Science (EECS), Gwangju Institute of Science and Technology, Gwangju 500-712, South Korea
*Corresponding author: ytlee@gist.ac.kr

Received 16 May 2016; revised 15 June 2016; accepted 16 June 2016; posted 17 June 2016 (Doc. ID 265255); published 14 July 2016

**This Letter reports a novel method for the simple fabrication of microlens arrays with a controlled shape and diameter on glass substrates. Multilayer stacks of silicon dioxide deposited by oblique angle deposition with hole mask patterns enable microlens formation. Precise control of mask height and distance, as well as oblique angle steps between deposited layers, supports the controllability of microlens geometry. The fabricated microlens arrays with designed geometry exhibit uniform optical properties.** 

***OCIS codes:*** (130.0130) Integrated optics; (220.0220) Optical design and fabrication.

http://dx.doi.org/10.1364/OL.41.003328

Microlenses are widely utilized for optical sensors [1–3], 3D display [4,5], lighting devices [6–11], microscopes [12,13], and solar cells [14] due to their advantages of small volume, light weight, and flexible design. Many methods have been developed to fabricate microlens, such as soft replica molding [15], laser-based patterning [16], ink-jet printing [17], and UV-nano imprint lithography [18]. Molding methods require a delicate mold, and available materials are limited to polydimethylsiloxane or polycarbonates. Also, these methods have a heat problem in the fabricating process and can be used for only array-based fabrication. To solve these problems, we present a new method of microlens manufacture that uses oblique angle deposition (OAD) by *e*-beam evaporation [19]. This OAD can solve the aforementioned problems. As using *e*-beam evaporation, microlens was made in the fabrication process. It means an individual microlens was used on a small optical device without arrangement. Also, the OAD method was elaborated by a microlens process to adjust the spherical lens. The OAD method can easily control the curvature of a microlens by changing the deposition angle of the substrate. In addition, any material can be deposited using an *e*-beam evaporator.

The material deposition area is affected by mask height shadowing for each oblique angle of incidence flux and is comprised of a circle shape by substrate rotation. By controlling the rotation of the substrate and the oblique angle flux for each angle, the size of a microlens can be changed. A material is partially deposited by the shadowing effect at oblique angles of 10° and 40° as illustrated in Fig. 1(a). Figure 1(b) shows a cross sectional SEM image of the photoresist mask and deposited silicon dioxide ($SiO_2$) layer. As the oblique angle is varied to 10°, 25°, and 40°, the deposit area is dramatically reduced.

Figure 2 shows the process of microlens fabrication using OAD for a convex lens. A negative photoresist (DNR-40, Donggin Semicam, Korea) was initially defined as a cylindrical hole pattern on a 2-inch glass wafer by conventional photolithography. The $SiO_2$ material layer was deposited on a substrate by an *e*-beam evaporator using inclined sample holders for tilted-angle evaporation. In addition, the substrate was rotated during the deposition sequence. The cylindrical hole pattern produced the shape of the microlens, which was obtained by the shadowing effect in the deposition of material. To produce the microlens with each incidence of oblique flux, the angle was gradually

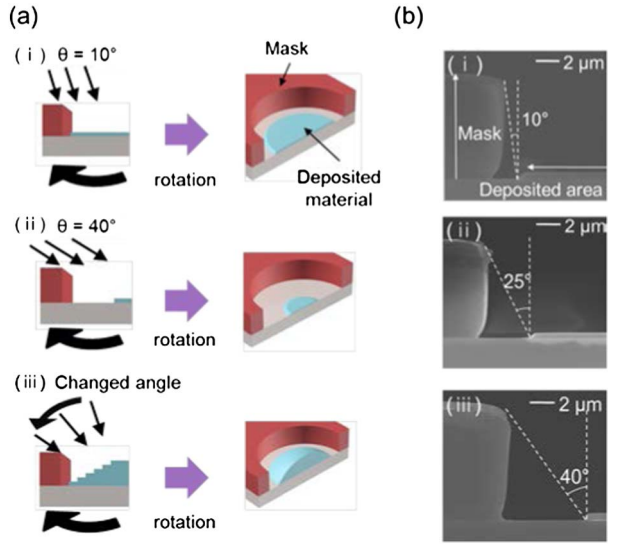


**Fig. 1.** (a) Schematic illustration of the oblique angle deposition process for the generation of microlenses: (i), (ii) material is partially deposited by shadowing effect at oblique angles of 10° and 40°, respectively; (iii) oblique angle is gradually changed from 5° to 60° with 12 steps. (b) Cross-sectional SEM images and deposited area: (i)–(iii) deposited area varies with each oblique angle of 10°, 25°, and 40°, respectively.

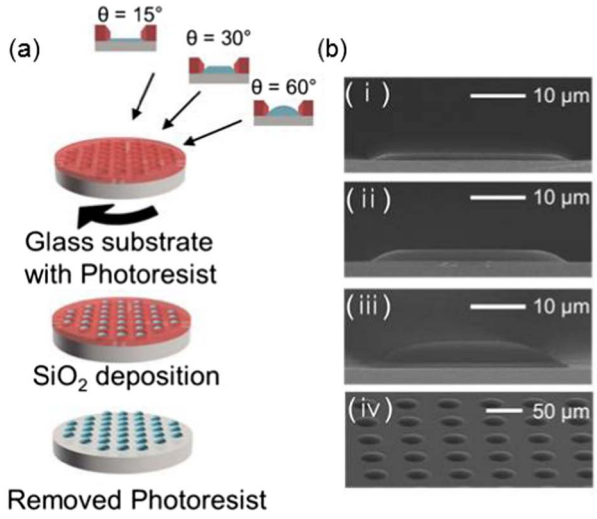


**Fig. 2.** (a) Schematic illustration of microlens fabrication process. (b) (i–iii) SEM image of a cross section microlens during material deposition at 15°, 30°, and 60°, respectively; (iv) SEM image of completed microlens.

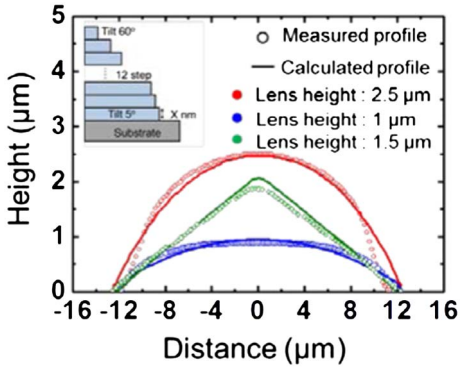


**Fig. 4.** Cross section profiles of fabricated and calculated lenses. Inset schematic shows each deposit layer. Microlens height was obtained according to number of steps and each layer $x$ nm height.

increased from 5° to 60°. Figure 2 shows cross sectional images of a material deposit from 5° to 15° [Fig. 2(b-i)], from 5° to 30° [Fig. 2(b-ii)], and from 5° to 60° [Fig. 2(b-iii)]. These results suggest that an adequate shape for a convex microlens can be generated when the OAD method provides a sufficient angle for mask size and height. Figure 3(a) shows the schematic of a microlens with mask pattern. The microlens size, i.e., the diameter $L$ and the height $H$ can be simply determined by the initial mask distance $L_M$, the mask height $H_M$, and oblique angle of incidence $\theta$. This relation can be expressed as [20]

$$L = L_M - \left[\frac{2H_M}{\{1 - \sin^2(90 - \theta)\}^{1/2}}\right]. \quad (1)$$

The calculated and measured lens diameter results are shown in Fig. 3(a) with a fixed mask height of 3 μm. The calculated lens diameter is similar to the measured value. On the other hand, the mask height and distance are important parameters to determine the lens diameter. A low height and a long mask distance could make a small shadow area, which would result in a large lens diameter as shown in Fig. 3(b). In other words, with a taller height and a shorter mask distance, the shadow area occupies the entire space. Also the oblique angle parameter must be considered in the OAD fabrication process. The maximum oblique angle was obtained in Eq. (1) by inserting zero for $L$ and by changing the mask distance [Fig. 3(c)]. For example, when the mask height was increased from 3 to 4 μm, the deposit area decreased from 9.77 to 7.96 μm. The results of which were limited by the incident maximum oblique angle evaporation beam on the substrate. The experimental results successfully demonstrate that the incident oblique angle was limited by the mask distance due to the decreased deposit area; therefore, the maximum angle of incidence differed for each lens size.

A refinement of microlens height can be accomplished using the deposit height of each angle layer. The profile resulting from variation of the deposit angle would be shaped like stairs. The total microlens height is determined by the number of deposited layer. In the deposit step, a fine structure having a smaller deposit angle interval is accomplished, resulting in a profile with smaller deviation. The measured surface profile and calculated profile of a microlens along a line passing through the center of the lens is shown in Fig. 4. To obtain a different curvature, it was changed to a deposition layer height thickness of 200 and 80 nm in the same diameter and same deposition steps. The blue dot profiles had a 1 μm height with 80 nm layers and 12 steps. The red dot profiles had a 2.5 μm height with 200 nm layers and 12 steps. To change the surface profile, the deposition layer thickness is dramatically decreased in each step. When the deposition layer thickness is increased

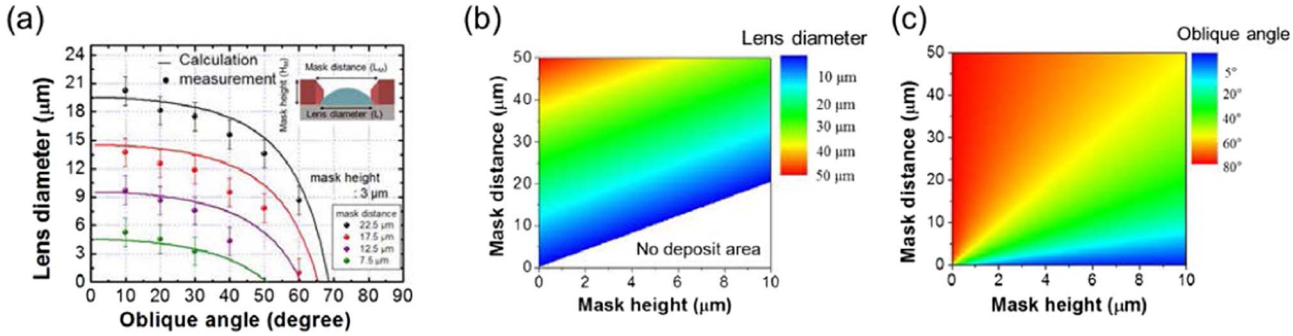


**Fig. 3.** (a) Experimentally measured and calculated lens size for mask sizes of 7.5, 12.5, 17.5, and 22.5 μm, respectively. (b), (c) Contour plots of calculated lens size and maximum oblique angle for related mask size and mask height.

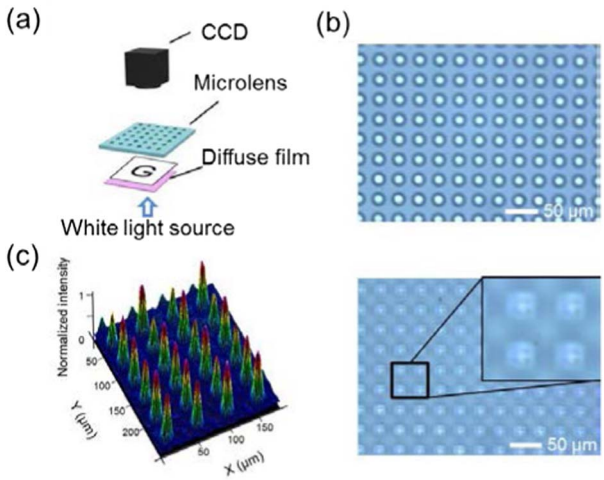


**Fig. 5.** (a) Schematic diagram of the optical microscope setup to obtain imaging and focusing performance of the microlens. (b) Image of the letter "G" obtained by using a microlens with 25 μm lens diameter and 2.5 μm lens height. (c) Measured light intensity profiles of microlens with 25 μm lens diameter and 2.5 μm lens height.

in each step, the surface profile obtained is that represented by the green dot profile in Fig. 4. As shown in the figure, deposition height control of each layer makes it possible to fabricate various microlenses, such as thin lenses, thick lenses, triangle lenses, etc. In between the measured and calculated profiles except for the error resulting from the *e*-beam evaporation, the fabricated microlenses were suitable for the width and height. The radius of curvature values of the fabricated microlenses were calculated from the circular fit to be 32.5 μm and 78.63 μm at 2.5 μm and 1 μm lens height, respectively.

The optical performance of microlenses produced using OAD was measured in terms of optical focal length and focusing performance. The lens transmission of convex microlenses was characterized with a white light source and a CCD camera to test its focusing and imaging properties. Each convex microlens was positioned horizontally on a motion stage and moved relative to the CCD camera. It was illuminated with a white light source from behind a paper with the pattern of the letter "G", which was printed on film. Figure 5(c) presents the view of the light intensity generated by each lens within the *xyz* plane passing through the microlens. Each microlens was characterized with a modified beam profile measurement system by imaging the optical section along a focusing beam under a laser beam at 760 nm. Light spots sharply focused on the false focal plane of the microlens could be obtained, with uniform normalized light intensity.

In summary, this work successfully demonstrated a new method of fabricating microlenses with controllable lens size by OAD. The lens shape can be precisely controlled by variation of the oblique angle and material deposit height. Furthermore, the microlens size is simply determined by the mask size and height during photolithography. The simple method can produce lenses of various sizes for single optical device applications, such as high-resolution imaging sensors, optical communication, projection systems, solid immersion lenses, and more. Moreover, other deposit materials, such as zinc sulfide, zinc oxide, and titanium dioxide, having different refractive indices, can be used replace $SiO_2$ to improve optical device performance.

**Funding.** Ministry of Trade, Industry and Energy (MOTIE) (20133010011750).

**Acknowledgment.** This work was supported by the New and Renewable Energy of the Korea Institute of Energy Technology Evaluation and Planning (KETEP) grant funded by the South Korean government Ministry of Trade, Industry and Energy.

## REFERENCES

1. P. Nussbaum, R. Völkel, H. P. Herzig, M. Eisner, and S. Haselbeck, Pure Appl. Opt. **6**, 617 (1997).
2. B. Stoklasa, L. Motka, J. Rehacek, Z. Hradil, and L. L. Sánchez-Soto, Nat. Commun. **5**, 3275 (2014).
3. H. Jung and K.-H. Jeong, Appl. Phys. Lett. **101**, 203102 (2012).
4. X. Xiao, B. Javidi, M. Martinez-Corral, and A. Stern, Appl. Opt. **52**, 546 (2013).
5. D. Lanman and D. Luebke, ACM Trans. Graph **32**, 220 (2013).
6. E. K. Kang, Y. M. Song, S. J. Jang, C. I. Yeo, and Y. T. Lee, IEEE Photon. Technol. Lett. **25**, 1118 (2013).
7. X.-H. Li, R. Song, Y.-K. Ee, P. Kumnorkaew, J. F. Gilchrist, and N. Tansu, IEEE Photon. J. **3**, 489 (2011).
8. X. H. Li, P. Zhu, G. Liu, J. Zhang, R. Song, Y. K. Ee, P. Kumnorkaew, J. F. Gilchrist, and N. Tansu, J. Display Technol. **9**, 324 (2013).
9. F. Galeotti, W. Mróz, G. Scavia, and C. Botta, Org. Electron. **14**, 212 (2013).
10. Y. K. Ee, P. Kumnorkaew, R. A. Arif, H. Tong, H. Zhao, J. F. Gilchrist, and N. Tansu, IEEE J. Sel. Top. Quantum Electron. **15**, 1218 (2009).
11. P. Zhu, G. Liu, J. Zhang, and N. Tansu, J. Display Technol. **9**, 317 (2013).
12. A. Orth and K. Crozier, Opt. Express **20**, 13522 (2012).
13. J. Kim, J.-H. Jung, Y. Jeong, K. Hong, and B. Lee, Opt. Express **22**, 10210 (2014).
14. Y. Chen, M. Elshobaki, Z. Ye, J.-M. Park, M. A. Noack, K.-M. Ho, and S. Chaudhary, Phys. Chem. Chem. Phys. **15**, 4297 (2013).
15. H.-T. Hsieh and G.-D. J. Su, J. Micromech. Microeng. **20**, 35023 (2010).
16. A. Tripathi, T. V. Chokshi, and N. Chronis, Opt. Express **17**, 19908 (2009).
17. S.-W. Tsai and Y.-C. Lee, J. Micromech. Microeng. **24**, 15014 (2014).
18. S. Tong, H. Bian, Q. Yang, F. Chen, Z. Deng, J. Si, and X. Hou, Opt. Express **22**, 29283 (2014).
19. S. J. Jang, Y. M. Song, J. S. Yu, C. I. Yeo, and Y. T. Lee, Opt. Lett. **36**, 253 (2011).
20. D. J. Poxson, F. W. Mont, M. F. Schubert, J. K. Kim, and E. F. Schubert, Appl. Phys. Lett. **93**, 101914 (2008).